Constant-Time Discontinuity Map for Forward Sensitivity Analysis to Initial Conditions: Spurs Detection in Fractional-N PLL as a Case Study

Federico Bizzarri, Angelo Brambilla, Alessandro Colombo
DEIB, Politecnico di Milano, Italy
Email: {fedrico.bizzarri, angelo.brambilla, alessandro.colombo}@polimi.it

Sergio Callegari
ARCES/DEI, University of Bologna, Italy
Email: sergio.callegari@unibo.it

***Abstract*—The constant-time discontinuity map is presented and used to compute the nonlinear effects of quantization noise injected in fractional$-N$ phase locked loops by $\Delta\Sigma$ modulators. The effects of quantization noise are studied through sensitivity analysis of the nominal trajectory of a noiseless integer$-N$ phase locked loop with respect to a small additive perturbation. It is shown that, to accurately measure the effects of quantisation noise injection, a simple linearized model is not sufficient. A nonlinear constant-time discontinuity map across the switching points of the vector field allows to improve the sensitivity analysis significantly, at a small computational cost.**

I. Introduction

The zero-time discontinuity map (ZDM) is well known in the area of hybrid dynamical system. In this paper, a generalization of the ZDM, that we referred to as constant-time discontinuity map (CT-DM), is introduced and exploited to efficiently and reliably compute the effects of quantization noise injected by $\Delta\Sigma$ modulators in fractional$-N$ phase locked loops (PLLs).

Sequences generated by the $\Delta\Sigma$ modulator can induce spurs in the output spectrum of the PLL mainly because of static and dynamic mismatch of the charge pump (CP) and its interaction with the digital delay usually present in the reset path of the phase frequency detector (PFD) [1]–[4]. These spurs are sequence-dependent and thus very difficult to compute since very time-consuming time-domain simulations must be performed in order to inject sufficiently long sequences (e.g., including more than 10^6 samples). Recently variational (i.e., linearized) models based on the *saltation matrix* were proposed to efficiently and reliably simulate effects of noise sources in PLLs [5] without resorting to macro-models. Unfortunately, despite providing accurate results, they are unable to correctly detect these spurs.

In this paper we present an advanced variational model based on the CT-DM. The basic idea is to resort to a standard, linearized model to simulate the system away from discontinuities, and to use a CT-DM to jump across discontinuities with sufficient numerical accuracy to correctly account for the fleeting nonlinear effects that are causing the spurs. The nonlinearity in the closed loop of the PLL manifests itself in the short time interval in which the action of the PFD and of the CP occurs. This results in a switching in the vector field. The linearization of the system dynamics at these points was done in [5] using the saltation matrix operator, i.e. the first order approximation of a ZDM. We show that by adopting a CT-DM and suitably increasing its order of approximation an efficient and accurate simulation tool can be obtained for fast testing of sequences of the $\Delta\Sigma$ modulator.

II. A primer on discontinuity maps

A discontinuous system is a tuple $\{X, Q, F, G, R\}$, where $X \subseteq \mathbb{R}^n$ is the space of the continuous variables $\boldsymbol{x}$; $Q \subseteq \mathbb{N}$ is a set of values for the discrete variable q; $F : X \times Q \to \mathbb{R}^n$ is a collection of smooth vector fields f_q; $G \subset X \times Q$ is a collection of discontinuity sets (or guards) each composed of possibly intersecting $(n-1)$-dimensional smooth manifolds in X , and $R : G \to X \times Q$ is a collection of reset maps. The vector fields f_q describe the system's evolution in each of the *domains* $q \in Q$, while guards and reset maps describe the rules of switching between domains. The *flow*

$$\phi(t, t_0, \boldsymbol{x}(t_0), q(t_0)) : \mathbb{R} \times X \times Q \to X \times Q \qquad (1)$$

is a map from $X \times Q$ to itself, parametrised in the time t.

Consider a ball $\mathcal{B}$ in X centered at $\boldsymbol{x}(t_0)$ and the set of initial conditions $(\mathcal{B}, q)$ for some fixed q, and consider a time t such that $\phi(t, t_0, \tilde{\boldsymbol{x}}(t_0), q(t_0))$ maps all initial states $(\tilde{\boldsymbol{x}}(t_0), q(t_0)) : \tilde{\boldsymbol{x}}(t_0) \in \mathcal{B}$ onto states with the same discrete variable q' in the (deformed) ball $\mathcal{B}'$. A ZDM M_0 for the set $(\mathcal{B}, q)$ and the time t is the map needed to verify the system of equations

$$\begin{aligned}&\phi(t, t_0, \tilde{\boldsymbol{x}}(t_0), q(t_0)) = \tilde{\boldsymbol{x}}(t) = \\ &\phi_2(t, t_1, \cdot, \cdot) \circ M_0 \circ \underbrace{\phi_1(t_1, t_0, \tilde{\boldsymbol{x}}(t_0), q(t_0))}_{\tilde{\boldsymbol{x}}(t_1)} \ ,\end{aligned} \qquad (2)$$

where ϕ_1 and ϕ_2 are flows of the smooth vector fields f_q and $f_{q'}$, respectively, and are assumed to be smoothly extended beyond the boundaries of their domains q and q'. In the literature, ZDMs have been studied and classified for many common discontinuity geometries. In a neighbourhood of a smooth portion of a guard, and away from points of tangency of the flow with G, the first-order approximation of a ZDM is known as the *saltation matrix* [6]. At points where the guard has a corner or is defined as the intersection of two smooth surfaces, the map is known to be continuous but nondifferentiable. Similarly, in the vicinity of points of tangency of the flow with the guard, the map is continuous, but can

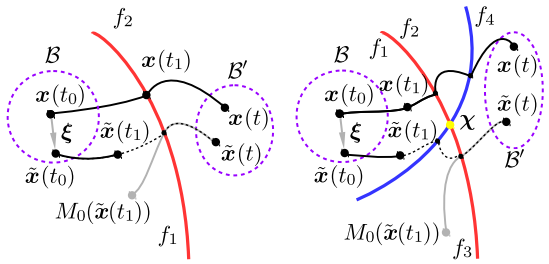

Figure 1. Sketchs of ZDMs. On the left, the ZDM is applied as soon as the reference trajectory reaches the guard whereas the perturbed trajectory is still in the domain q. On the right, the choice of t_1 is more generic.

be differentiable or not depending on the geometry the flow around the discontinuity [6], [7].

A sketch of a typical ZDM is depicted in the left part of Fig. 1 where a (reference) trajectory originated at $\boldsymbol{x}(t_0)$ leaves a domain $q = 1$ and enters a domain $q' = 2$. Given any small perturbation $\boldsymbol{\xi}$ of $\boldsymbol{x}(t_0)$, the ZDM is the map that has be applied to $\tilde{\boldsymbol{x}}(t_1)$ in the domain q so that, by simply integrating $M_0(\tilde{\boldsymbol{x}}(t_1))$ in the flow of $f_{q'}$, one obtains the correct integral once the trajectory reaches the domain q'. A more complex example ($q = 1$ and $q' = 4$) is reported in the right part of Fig. 1, where the reference trajectory reaches two consecutive guards near their intersection point $\boldsymbol{\chi}$. In this case, it may happen that the perturbed trajectory hits the manifolds in the inverse sequence (with respect to the reference trajectory) and the ZDM must be computed taking into account that initial conditions in $\mathcal{B}$ may behave differently depending on the order with which they reach the guards.

In principle Eq. (2) can be modified in order to apply the ZDM directly at $\tilde{\mathbf{x}}(t_0)$ obtaining

$$\phi(t, t_0, \tilde{\boldsymbol{x}}(t_0), q(t_0)) = \phi_2(t, t_0, \cdot, \cdot) \circ M_0 \circ \tilde{\boldsymbol{x}}(t_0) \quad . \tag{3}$$

An example is reported in Fig. 2 for a trajectory reaching three consecutive guards ($q = 1$ and $q' = 5$).

An extension of the ZDM is obtained modifying Eq. (2) as

$$\begin{aligned} &\phi(t, t_0, \tilde{\boldsymbol{x}}(t_0), q(t_0)) = \\ &\quad \phi_2(t, t_1 + \delta t, \cdot, \cdot) \circ M_{\delta t} \circ \phi_1(t_1, t_0, \tilde{\boldsymbol{x}(t_0)}, q(t_0)) \quad , \end{aligned} \tag{4}$$

with $\delta t \in \mathbb{R}$. We call this the *constant-time discontinuity map* (CT-DM). An example of such a map is depicted in Fig. 2 in the case $t_1 = t_0$. It is worth mentioning that if

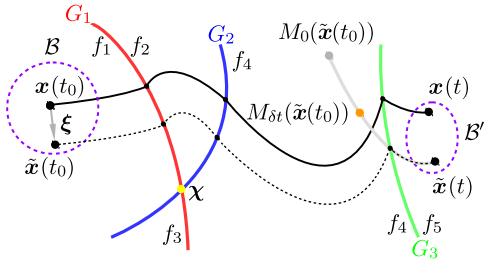

Figure 2. The ZDM $M_0(\cdot)$ is applied directly in $\mathcal{B}$. The solid dot corresponding to $M_{\delta t}(\tilde{\boldsymbol{x}}(t_0))$ represent a CT-DM applied to initial conditions in $\mathcal{B}$.

$\delta t = t - t_0$, then $M_{t-t_0}(\tilde{\boldsymbol{x}}(t_0))$ maps $\tilde{\boldsymbol{x}}(t_0)$ directly in $\tilde{\boldsymbol{x}}(t)$. Note that the derivation of the CT-DM for typical discontinuity geometries remains formally equivalent to the corresponding ZDM, and shares the same smoothness properties. For a given dynamical system, a sufficiently differentiable CT-DM can be computed numerically, by identifying the coefficients of its Taylor expansion

$$M_{\delta t}(\boldsymbol{x} + \boldsymbol{\xi}) := M_{\delta t}|_{\boldsymbol{x}} + DM_{\delta t}|_{\boldsymbol{x}}\, \boldsymbol{\xi} + \dots \quad , \tag{5}$$

where $D\cdot$ is the differential of $\cdot$ in $\boldsymbol{x}$.[1] For a given $\boldsymbol{x}$, the coefficients of the above expansion can be identified by least squares, after having computed a sufficiently large number of pairs $(M_{\delta t}(\boldsymbol{x} + \boldsymbol{\xi}), \boldsymbol{\xi})$ by numerical integration.

III. Trajectory sensitivities with respect to initial conditions using the CT-DM

Consider a generic discontinuous system $\{X, Q, F, G, R\}$ where F is assumed autonomous and G time-invariant, and indicate $\boldsymbol{\gamma}$ as a periodic orbit of the system. This is fully general, as any nonautonomous F can be rewritten as autonomous (time-dependent) once the open loop input signal or the feedback law have been designed, and any time-variant G is rewritten as time-invariant by adding time to the state variables.

The behaviour of small perturbations to a trajectory through the flow of F can be easily studied using the *fundamental solution matrix*: given the flow $\phi(t, t_0, \boldsymbol{x}(t_0), q(t_0))$, it is the matrix $\Psi(t, t_0)$ of partial derivatives of the flow with respect to $\boldsymbol{x}(t_0)$, evaluated at $(\boldsymbol{x}(t), q(t))$. Even if $\boldsymbol{x}(t_0)$ and $q(t_0)$ are parameters of the fundamental solution matrix, to keep the notation simple we will not state them explicitly. The fundamental solution matrix maps infinitesimal perturbation of $\boldsymbol{x}(t_0)$ to infinitesimal perturbations of $\boldsymbol{x}(t)$.

During a time interval $[t_0, t]$, when the system remains in a single domain q, $\boldsymbol{\gamma}$ is a solution of a smooth vector field $f_q(\boldsymbol{x}, t)$, and the fundamental solution matrix can be computed as the solution of the variational problem

$$\dot{\Psi}(t, t_0) = J_q(\boldsymbol{x}, t)\Psi(t, t_0), \quad \Psi(t_0, t_0) = I, \tag{6}$$

where J_q is the Jacobian of f_q and I is the identity matrix. A sufficiently small perturbation $\boldsymbol{\xi}(t_0)$ to an initial condition $\boldsymbol{\gamma}(t_0)$ is then mapped by the flow of f_q through the map

$$\boldsymbol{\xi}(t) = \Psi(t, t_0)\boldsymbol{\xi}(t_0) + O(\|\boldsymbol{\xi}\|^2). \tag{7}$$

Typically, away from discontinuities and strong nonlinearities, the first-order approximation of the above map is sufficient to capture the behaviour of small perturbations of $\boldsymbol{\xi}(t)$, so that the fundamental solution matrix is all that is needed. When the flow crosses a discontinuity (or a strong nonlinearity) during the interval $[t_0, t]$, the above equation can be rewritten in terms of a CT-DM (with constant time $\delta t = t - t_0$) as

$$\boldsymbol{\xi}(t) = M_{t-t_0}(\boldsymbol{x}(t_0) + \boldsymbol{\xi}(t_0)) - \boldsymbol{x}(t) + O(\|\boldsymbol{\xi}(t_0)\|^{\zeta+1}), \tag{8}$$

[1]Though (5) is defined only for a differentiable CT-DM, in the example at the end of this paper it will be numerically applied in a nonsmooth case. We will show that, despite being formally not correct, in our case study it provides an excellent result.

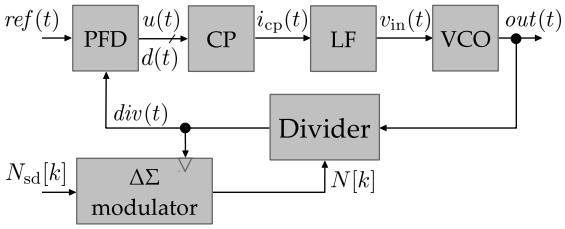

Figure 3. Fractional$-N$ PLL architecture.

where ζ is the approximation order of the CT-DM.

The advantage of computing the above map, instead of integrating the flow, is that the CT-DM is computed once, analytically, or approximated numerically, and then used as a static map to integrate the small signal through nonlinearities and discontinuities. To determine the effects of a small perturbation to an initial condition it is thus sufficient to iterate the linear map (7) and the nonlinear map (8).

IV. A CASE STUDY

The onset of spurs in fractional$-N$ PLL is mainly due to static and dynamic mismatch of the CP and its interaction with the digital delay usually present in the reset path of the PFD [1]–[4]. The nonlinearity arising from this interaction acts in a short interval of the PLL reference-signal period and consequently the proposed approach can be exploited to derive a more accurate small-signal model of the PLL dynamics than a simple first order one, adequate to grasp the nonlinear effects causing fractional spurs. We consider a Type-II wide-band fractional$-N$ PLL (see the block schematic in Fig. 3) charaterized by a closed loop bandwidth $f_0 = 1\,\mathrm{MHz}$, $f_{\mathrm{ref}} = {}^1\!/_{T_{\mathrm{ref}}} = 50\,\mathrm{MHz}$ and $N_{\mathrm{int}} = 72$ (as in [8]). The parameter values of the loop filter (LF) (see Fig. 4 and Tbl. I) are derived according [9]. The transfer function $G(s)$ is of 2$^{\mathrm{nd}}$ Butterworth

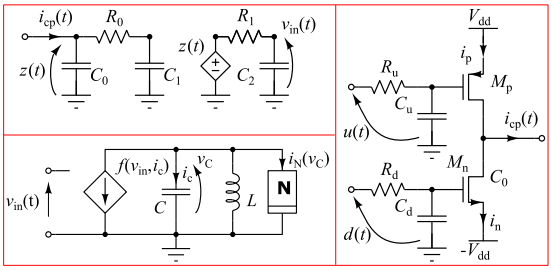

Figure 4. Upper left panel: The LF. Component parameters as in Tbl. I. Lower left panel: The VCO. $C = 2\,\mathrm{pF}$ and $L = 0.9772\,\mathrm{nH}$ are such that $f_{\mathrm{VCO}} = f_{\mathrm{ref}} N_{\mathrm{int}} = 3.6\,\mathrm{GHz}$ if $v_{\mathrm{in}} = 0$. $i_{\mathrm{N}}(v_{\mathrm{C}}) = a_7 v_{\mathrm{C}}^7 + a_5 v_{\mathrm{C}}^5 + a_3 v_{\mathrm{C}}^3 + a_1 v_{\mathrm{C}}$ where $a_7 = -8.9641\times10^{-7}$, $a_5 = 2.5834\times10^{-5}$, $a_3 = -1.5571\times10^{-4}$, $a_1 = -6.3524\times10^{-5}$, and $f(v_{\mathrm{in}}, i_{\mathrm{c}}) = \beta v_{\mathrm{in}} i_{\mathrm{c}}$ with $\beta = -0.1157\,\mathrm{V}^{-1}$. Right panel: The MOSFET CP. The component parameters are reported in Tbl. I. For the transistors a Level-1 model is assumed. The logic levels of the ideal square waveforms $u(t)$ and $d(t)$, respectively, are $V_{\mathrm{dd}}/2$ (high logic level) and V_{dd} (low logic level) and $-V_{\mathrm{dd}}/2$ (high logic level) and $-V_{\mathrm{dd}}$ (low logic level).

Table I
DEFINITION OF PARAMETERS FOR THE LF AND CP CIRCUITS IN FIG. 4.

C_0	$\frac{f_z}{K_{\mathrm{LP}} f_p}$	C_1	$\frac{f_p - f_z}{K_{\mathrm{LP}} f_p}$	C_2	$\frac{1}{2\pi R_1 f_{ps}}$
R_0	$\frac{1}{2\pi C_1 f_z}$	R_1	$1\,\mathrm{k\Omega}$	R_u	$1\,\mathrm{k\Omega}$
R_d	$1\,\mathrm{k\Omega}$	C_u	$300\,\mathrm{fF}$	C_d	$100\,\mathrm{fF}$
V_{dd}	$3\,\mathrm{V}$	v_T	$0.5\,\mathrm{V}$	λ	2×10^{-5}
$k_{\{p,n\}}$	$\frac{(1+\mu_{\{p,n\}})I_{\mathrm{cp}}}{(0.5V_{\mathrm{dd}}-V_T)^2}$	μ_p	0.01	μ_n	-0.01

type, i.e.,

$$G(s) = \underbrace{K\frac{N_{\mathrm{int}} + N_{\mathrm{frac}}}{K_{\mathrm{VCO}} I_{\mathrm{cp}}}}_{K_{\mathrm{LP}}} \frac{1 + \frac{s}{2\pi f_z}}{s\left(1 + \frac{s}{2\pi f_p}\right)} \quad ,$$

with $N_{\mathrm{frac}} = -2\times10^{-10}$, $K_{\mathrm{VCO}} = 210\,\mathrm{MHzV}^{-1}$, $K = 2.885\times10^{12}$, $f_p = 2.807\,\mathrm{MHz}$, $f_z = {}^1\!/_9 f_0$, $f_0 = 1\,\mathrm{MHz}$. The nominal value I_{cp} for both the up and down current sources of the CP is set to $5\,\mathrm{mA}$. The pole at $f_{ps} = 2.5\,\mathrm{MHz}$ of the original design [8] is implemented through the C_2 capacitor and the R_1 resistor. The VCO (see Fig. 4) is modelled as a modified version of the Van der Pol oscillator [5]. The parallel connection of a nonlinear controlled current-source and of the capacitor C forms an equivalent voltage-controlled linear capacitor that allows the oscillator to be tuned.

The CP is modeled as in Fig. 4 where i_{p} and i_{n} are both statically and dynamically mismatched to account for different transconductance and equivalent gate capacitance of the PMOS and NMOS transistors. The PFD analog mixed signal (AMS) circuit, characterized by the typical tristate architecture [5], [9], drives the CP through the signals $u(t)$ and $d(t)$. The former switches from its low logic level to the high one whenever a positive edge of the $ref(t)$ signal is detected. The latter does the same according to the transitions of $div(t)$. These events correspond to discontinuities of the vector field governing the PLL. If at $t = \bar{t}$ both these signals are simultaneously at their high logic level, a delayed event is scheduled at $\bar{t} + t_d$ to reset them to low logic level. We take $t_d = 100\,\mathrm{ps}$.

Following a procedure discussed in [5], the model in Fig. 3 can be rewritten as an equivalent model where the $\Delta\Sigma$ modulator block is removed, and $ref(t)$ is substituted with a signal $ref(t + \varphi(t))$, where $\varphi(t)$ is a time-dependent phase offset. The phase offset affects the system dynamics only by changing the time of switching of the signal $u(t)$, therefore, it enters the model as a time-dependent guard. To formulate the model with time-independent guards, we define the state $\boldsymbol{x}$ to include the state variables of the PLL, *plus* the variable φ. The equivalent model is thus described as

$$\begin{pmatrix} \dot{\boldsymbol{x}}(t) \\ \dot{\varphi}(t) \end{pmatrix} = \begin{pmatrix} F(\boldsymbol{x}(t), q(t)) \\ 1 \end{pmatrix} + \begin{pmatrix} 0 \\ \beta(t) \end{pmatrix} \quad ,$$

where

$$\beta(t) = \sum_k \frac{2\pi\left(n[k] - N_{\mathrm{frac}} T_{\mathrm{ref}}\right)}{N_{\mathrm{int}} + N_{\mathrm{frac}}} \delta(t - t_0 - kT_{\mathrm{ref}}) \quad . \qquad (9)$$

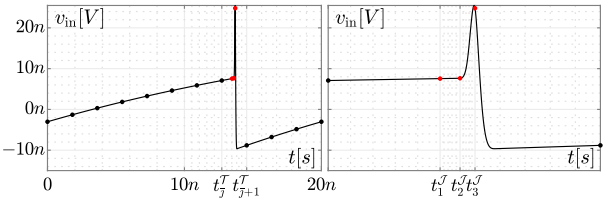

Figure 5. In the left panel the steady-state evolution of the $v_{\rm in}(t)$ signal tuning the VCO is reported. Black dots represent the samples obtained choosing $N_{\mathcal{T}} = 11$. In the right panel an enlargement showing the time instants corresponding to discontinuities of the vector field.

In Eq. (9), $n[k] = N[k] - (N_{\rm int} + N_{\rm frac})$, i.e. it is the running difference between the current value of the frequency division ratio set by the $\Delta\Sigma$ modulator and the nominal fractional division ratio of the PLL, which is constant during the $k-$th working period of the system.

This approach grounds on [9], where a small-signal equivalent source is introduced to model, in the frequency domain, the effects of quantisation noise as jitter acting on $div(t)$. Here, since the PFD dynamics is governed by the relative position of the (rising) edges of $ref(t)$ and $div(t)$, the jitter is moved to the phase of the former thus considering the fractional$-N$ PLL as if it were an integer$-N$ one and then altering its reference signal instead of its frequency division ratio.

It is crucial to notice that the train of $\delta(\cdot)$ functions in (9) acts on the variable φ by instantaneously resetting its current value, that remains constant from one $\delta(\cdot)$ to the next. Consequently it is possible to view $\beta(t)$ as a sequence of perturbations to the state of the system occurring once in any working period of the integer$-N$ PLL. To determine their effect we can study the sensitivity of the steady state solution of the circuit with respect to perturbations of its initial conditions.

By resorting to an improved version of the time-domain shooting method [10], [11] the periodic steady state solution $\boldsymbol{\gamma}(t) = (\boldsymbol{x}_s, \varphi_s)^{\rm T}$ of the integer$-N$ PLL in the $[t_0, t_0 + T_{\rm ref}]$ time interval is computed (see Fig. 5) and stored at $N_{\mathcal{T}} + 1$ evenly-spaced time-samples $t_j^{\mathcal{T}}$ $(j = 0, \ldots, N_{\mathcal{T}})$. Furthermore the $N_{\mathcal{J}}$ time instants $t_l^{\mathcal{J}}$ $(l = 1, \ldots, N_{\mathcal{J}})$ corresponding to discontinuities in the vector field are introduced. The index $j = \bar{\jmath}$ such that $t_l^{\mathcal{J}} \in [t_{\bar{\jmath}}^{\mathcal{T}}, t_{\bar{\jmath}+1}^{\mathcal{T}}]$ for $l = 1, \ldots, N_{\mathcal{J}}$ is identified and the CT-DM $M_{t_{\bar{\jmath}+1}^{\mathcal{T}} - t_{\bar{\jmath}}^{\mathcal{T}}}(\cdot)$ is approximated by a Taylor

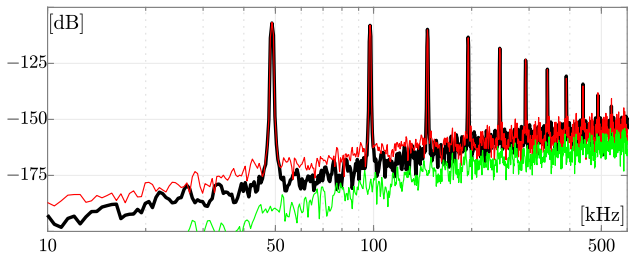

Figure 6. The PSD of the $v_{\rm in}(t)$ voltage obtained by resorting to a large-signal simulation (in black) and to the proposed method ($N_{\mathcal{T}} = 11$) for $\zeta = 1$ (in red) and $\zeta = 3$ (in green).

polynomial of order $\zeta = 3$. The matrices $\boldsymbol{\Psi}(t_j^{\mathcal{T}}, t_{j-1}^{\mathcal{T}})$, for $j = 1, \ldots, N_{\mathcal{T}}$ and $j \neq \bar{\jmath}$, are obtained by solving the variational problem (7) associated to $\boldsymbol{\gamma}(t)$ in each time interval $[t_{j-1}^{\mathcal{T}}, t_j^{\mathcal{T}}]$ choosing $\boldsymbol{\Psi}(t_{j-1}^{\mathcal{T}}, t_{j-1}^{\mathcal{T}}) = I$. The $\beta(t)$ signal in (9) is that of the MASH 1-1 $\Delta\Sigma$ modulator sequence used in [4]. Assuming $t_0 = 0$, the effect of $\beta(t)$ and consequently of the quantization noise inherent in the sequence originating it, was computed for 5×10^5 working periods of the PLL by iterating the map

$$\begin{pmatrix} \boldsymbol{\xi}_{\boldsymbol{x}} \\ \xi_\varphi \end{pmatrix}_{k+1} = \prod_{j=\bar{\jmath}+1}^{N_{\mathcal{T}}+1} \boldsymbol{\Psi}(t_j^{\mathcal{T}}, t_{j-1}^{\mathcal{T}}) \cdot$$

$$\cdot \left[M_{t_{\bar{\jmath}}^{\mathcal{T}} - t_{\bar{\jmath}-1}^{\mathcal{T}}} \left(\prod_{j=1}^{\bar{\jmath}} \boldsymbol{\Psi}(t_j^{\mathcal{T}}, t_{j-1}^{\mathcal{T}}) \cdot \begin{pmatrix} \boldsymbol{\xi}_{\boldsymbol{x}} \\ \xi_\varphi + \beta \end{pmatrix}_k \right) - \boldsymbol{\gamma}(t_{\bar{\jmath}}) \right],$$

where the notation $(\cdot)_k$ means that $(\cdot)$ is computed in $t = kT_{\rm ref}$, $\boldsymbol{\xi}_{\boldsymbol{x}}$ and ξ_φ represent deviation from the steady state solution components $\boldsymbol{x}_s$ and φ_s, respectively. The power spectral density (PSD) of the component of $\boldsymbol{\xi}_{\mathbf{x}}$ corresponding to the $v_{\rm in}(t)$ signal tuning the VCO is plotted in Fig. 6 with the PSD of the signal obtained by performing a transient simulation of the fractional$-N$ PLL for the same number of working periods. The result of the proposed method with $\zeta = 1$ is also shown. This highlights how a simple linearisation of the steady state dynamics does not capture the presence of spurs and underestimates the effects of quantization noise.

References

[1] H. Arora, N. Klemmer, J. Morizio, and P. Wolf, "Enhanced phase noise modeling of fractional-N frequency synthesizers," *Circuits and Systems I, IEEE Trans. on*, vol. 52, no. 2, pp. 379–395, Feb 2005.

[2] H. Hedayati, B. Bakkaloglu, and W. Khalil, "Closed-loop nonlinear modeling of wideband $\Sigma\Delta$ fractional-N frequency synthesizers," *Microwave Theory and Techniques, IEEE Transactions on*, vol. 54, no. 10, pp. 3654–3663, Oct 2006.

[3] K. Hosseini, B. Fitzgibbon, and M. Kennedy, "Observations concerning the generation of spurious tones in digital $\Delta\Sigma$ modulators followed by a memoryless nonlinearity," *Circuits and Systems II: Express Briefs, IEEE Transactions on*, vol. 58, no. 11, pp. 714–718, Nov 2011.

[4] E. Familier and I. Galton, "Second and third-order noise shaping digital quantizers for low phase noise and nonlinearity-induced spurious tones in fractional-N PLLs," *IEEE Transactions on Circuits and Systems I*, vol. 63, no. 6, pp. 836–847, June 2016.

[5] F. Bizzarri, A. Brambilla, and G. Storti Gajani, "Periodic small signal analysis of a wide class of Type-II Phase Locked Loops through an exhaustive variational model," *Circuits and Systems I, IEEE Transactions on*, vol. 59, pp. 2221 – 2231, 2012.

[6] M. Di Bernardo, C. Budd, A. Champneys, and P. Kowalczyk, *Piecewise-smooth Dynamical Systems, Theory and Applications*. Springer-Verlag, 2008.

[7] A. Colombo, "Boundary intersection crossing bifurcation in the presence of sliding," *Physica D*, vol. 237, pp. 2900–2912, 2008.

[8] S. E. Meninger, "Design of a wideband fractional-N frequency synthesizer using CppSim," 2008. [Online]. Available: http://www.cppsim.com/Tutorials/wideband_fracn_tutorial.pdf

[9] M. Perrott, M. Trott, and C. Sodini, "A modeling approach for $\Sigma\Delta$ fractional-N frequency synthesizers allowing straightforward noise analysis," *Solid-State Circuits, IEEE Journal of*, vol. 37, no. 8, pp. 1028–1038, Aug 2002.

[10] F. Bizzarri, A. Brambilla, and G. Storti Gajani, "Steady state computation and noise analysis of analog mixed signal circuits," *Circuits and Systems I, IEEE Transactions on*, vol. 59, no. 3, pp. 541 – 554, Mar. 2012.

[11] ——, "Extension of the variational equation to analog/digital circuits: numerical and experimental validation," *International Journal of Circuit Theory and Applications*, vol. 41, no. 7, pp. 743–752, 2013.